J Solid State Electrochem (2003) 7: 91 – 105
DOI 10.1007/s10008-002-0316-1

ORIGINAL PAPER

Enn Lust · Gunnar Nurk · Alar Jänes · Mati Arulepp
Priit Nigu · Priit Möller · Silvar Kallip
Väino Sammelselg

Electrochemical properties of nanoporous carbon electrodes in various nonaqueous electrolytes

Received: 2 November 2001 / Accepted: 12 April 2002 / Published online: 23 October 2002

Abstract Electrical double layer and electrochemical characteristics at the nanoporous carbon|acetonitrile interface with additions of Et_4NBF_4, Et_3MeNBF_4, $EtMe_3NBF_4$, $LiClO_4$, and $LiBF_4$ have been studied by cyclic voltammetry and impedance spectroscopy methods. A value of zero charge potential, dependent on the structure of the cations as well as on the composition of the anions, the region of ideal polarizability, and other characteristics has been established. Analysis of the complex plane plots shows that the nanoporous carbon|acetonitrile + 0.1 M electrolyte (Et_4NBF_4, Et_3MeNBF_4, or $EtMe_3NBF_4$) interface can be simulated by the equivalent circuit, in which the two parallel conduction parts in the solid and liquid phases are interconnected by the double layer capacitance in parallel with the complex admittance of the hindered reaction of the charge transfer process or of the partial charge transfer (i.e. adsorption stage limited) process. The values of the characteristic frequency depend on the electrolyte composition and on the electrode potential, i.e. on the nature of the ions adsorbed at the surface of the nanoporous carbon electrode. In the region of moderate a.c. frequencies, the modified Randles-like equivalent circuit has been used for simulation of the complex plane plots. In the region of negative surface charge densities, the intercalation process of Li^+ ions from $LiClO_4$ and $LiBF_4$ solutions into the surface film is possible and these data can be simulated using the modified Ho et al. model or Meyer et al. model.

Keywords Electrical double layer · Nanoporous carbon · Zero charge potential · Nonaqueous electrolyte solution

Presented at the Regional Seminar on Solid State Ionics, Jūrmala, Latvia, 22–26 September 2001

E. Lust (✉) · G. Nurk · A. Jänes · M. Arulepp · P. Möller
Institute of Physical Chemistry, University of Tartu,
2 Jakobi Str., 51014 Tartu, Estonia
E-mail: enn@chem.ut.ee

E. Lust · G. Nurk · A. Jänes · M. Arulepp · P. Nigu · P. Möller
Tartu Technologies Ltd., 185 Riia Str.,
51014 Tartu, Estonia

S. Kallip
Institute of Physical Chemistry, University of Tartu,
2 Jakobi Str., 51014 Tartu, Estonia

V. Sammelselg
Institute of Physics, University of Tartu,
142 Riia Str., 51014 Tartu, Estonia

Introduction

The electrochemical and electrical double layer characteristics of carbon electrodes have been studied for a long time, but there are many problems which have not been solved at the moment [1, 2, 3, 4, 5, 6, 7, 8, 9, 10, 11, 12, 13, 14, 15]. Electric double layer characteristics of various carbonaceous materials are very important, as these parameters determine the electrical behaviour of the electrical double layer capacitors (EDLCs), where the electrical charge is stored in the double layer (as the Gibbs energy of adsorption) and is based mainly on electrostatic interactions (so-called physical adsorption). As the electrostatic interactions are significantly less detrimental to electrodes and to solution stability than the usual electrochemical redox reactions, used for the generation of electricity in fuel cells as well as in various batteries, EDLCs can be recharged -discharged up to 10^6 times. The very important advantages of EDLCs are their reversibility and the comparatively low temperature coefficient [1]. However, a very important problem with EDLCs is their relatively low energy density compared with rechargeable batteries. It is well known that the performance specifications of an electrochemical capacitor, e.g. in terms of the relations between achieved power densities and corresponding energy densities, depend on the equivalent series resistance (ESR) and on the internal distribution of electrode resistance (IER) in the pore matrix of the electrodes [1, 2, 3, 4, 5].

The capacitance of EDLCs depends mainly on the specific surface area of the carbon material used for preparation of the electrodes. Theoretically, the higher the surface area of the activated carbon, the higher the specific capacitance expected (the specific capacitance is defined as the specific surface area of carbon multiplied by the double layer capacitance C_{dl} (F cm^{-2}) [1]). However, the practical situation is more complicated and usually the capacitance measured does not have a linear relationship with the specific surface area of the electrode material. There are two main reasons for this phenomenon: (1) the double layer capacitance varies with various types of activated carbon that are made from different types of precursors (through different processes and subsequent treatments) [1, 2, 3, 4, 5, 6]; (2) nanopores with a small diameter may not be accessible to the electrolyte solution simply because the electrolyte ions, especially large organic ions and ions with a hydration cell, are too large to enter into the nanopores. Thus, the surface area of these non-accessible nanopores will not contribute to the total double layer capacitance of the electrode material.

It should be noted that in the literature there are very large differences between the values of the electric double layer capacitance of carbonaceous materials, ranging from 3 μF cm^{-2} for the basal plane of stress-annealed highly oriented pyrolytic graphite (HOPC) to 70 μF cm^{-2} for the polished graphite edge plane [1, 2, 3, 16, 17]. This surprisingly low non-faradaic differential capacitance value for the $C(0001)$ plane compared with the capacitance values for metals (18–20 μF cm^{-2} for Hg, Bi and Cd [18]), having almost parabolic dependence on the electrode potential, can be explained on the basis that a substantial fraction of the potential drop between the solid electrode and the solution occurs in a space charge layer within the carbonaceous material. In the 1970s and 1980s, various physical models were introduced into electrochemistry, taking into account the potential drop in the thin surface layer of the electrode [16, 17, 18, 19, 20, 21]. However, those models cannot be used for the interpretation of the experimental impedance data for porous carbonaceous materials because the surface roughness factor at porous electrodes is not a very well established parameter. In any case, the potential drop in the thin surface layer of carbonaceous materials is very important [1, 2, 16, 17, 18].

It should be noted that carbonaceous materials show a frequency-dependent capacitance even through the capacitance should be independent of frequency. This abnormal frequency dependence is called a distributed characteristic or "frequency dispersion" of the electrical properties [1, 2, 3, 4, 5, 6, 7, 8, 9, 10, 11, 12, 13, 14]. A circuit element with the distributed characteristic cannot be exactly expressed as a combination of a finite number of ideal circuit elements, except in certain limiting cases. The distributed characteristic results mainly from two origins [1, 2, 3, 4, 5, 6, 7, 8, 9, 10, 11, 12, 13, 14, 15]:

1. It appears non-locally when a dimension of a system under study (electrode thickness or pore length) is longer than the characteristic length (for example, diffusion length or a.c. penetration depth), which is a function of frequency. This type of distributed characteristic exits even when all the system properties are homogeneous and space invariant (double layer charging of a porous electrode, diffusion in diffusion-limited systems, adsorption of anions and cations, surface reconstruction and transformation in the adlayers).
2. The distributed characteristic is attributed to various heterogeneities: geometric inhomogeneity, such as the surface roughness or the distribution of pore size, as well as the crystallographic anisotropy and the surface disorder of a polycrystalline electrode.

Theoretical background

Beginning essentially with the work of de Levie [10, 12, 13], a large number of various models have been developed [1, 2, 8, 9, 11, 14, 15, 16, 17] to describe theoretically the experimental behaviour of the carbon or porous carbon electrodes. A very important direction is the investigation of the influence of the pore geometry on the data for impedance spectroscopy (EIS) [14, 15]. Some authors use simple modifications of the classical Randles-Frumkin-Melik-Gaikazyan equivalent circuits [22, 23, 24], involving a constant phase element or Warburg diffusion impedance modified according to the boundary conditions [1, 8, 25, 26], as well as branched transmission line equivalent circuits [1, 8, 27]. Paasch et al. [11] developed a theory for a macroscopically homogeneous porous electrode, where three main processes are considered: (1) ionic conductivity in the pore electrolyte and electronic conductance in the electrode (solid) phase; (2) charging the double layer at the solid|liquid interface; and (3) a simple charge transfer reaction (c.t.r.) at the interface or the partial c.t.r. for the ideally polarizable electrode [28]. The averaged polarization at the porous surface was described by a diffusion equation, with the linear source term representing the c.t.r. This leads to polarization of the porous electrode. According to this theory, the position- (x) and time- (t) dependent polarization ($\tilde{E}(x,t)$) (averaged for the porous surface) is given as (without regard to an unknown constant):

$$\tilde{E}(x,t) \equiv \phi_1 - \phi_2 \tag{1}$$

where ϕ_1 is a value of potential in the solid phase (taken independent of x, $\phi_1 \neq f(x)$) [11]. The potential in the pore electrolyte ϕ_2 is determined by its conductivity, double layer formation parameters and c.t.r. characteristics of the interface (or by the partial charge transfer characteristics for an ideally polarizable electrode). Averaging this potential over the volume element,

containing many pores, gives the position- and time-dependent potential ($\phi_2(x,t)$). The basic equation of the macro-homogeneous theory for the case of a constant concentration of the electrolyte is given as:

$$C_1\frac{\partial\tilde{E}}{\partial t}=-\frac{1}{r_2}\frac{\partial^2\phi_2}{\partial x^2}+AS_{\mathrm{p}}j_0 \left\{\exp\left[\frac{-\alpha nF}{R_{\mathrm{g}}T}(\tilde{E}-E_{\mathrm{t}})\right]-\exp\left[\frac{(1-\alpha)nF}{R_{\mathrm{g}}T}(\tilde{E}-E_{\mathrm{t}})\right]\right\} \tag{2}$$

where E_{t} is the equilibrium polarization, R_{g} is the universal gas constant, and C_1 is the double layer capacitance per unit length (averaged similarly to the potential):

$$C_1=AS_{\mathrm{p}}C_{\mathrm{dl}} \tag{3}$$

where C_{dl} is the universal double layer capacitance per unit area A; S_{p} is the area of the pores per unit volume, on which a double layer can be formed [9, 11]. Further, $r_2=\rho_2/A$ denotes the electrolyte resistance per unit length in the pore and:

$$\rho_2=\rho_2*f_{\mathrm{p}}/v_{\mathrm{p}} \tag{4}$$

where ρ_2 is the electrolyte resistivity per unit length in the pore, ρ_2* is the bulk electrolyte resistivity, f_{p} is the tortuosity factor [29] and v_{p} is the relative pore volume. The term in braces in Eq. 2 is due to the averaged faradaic current at the pore surfaces corresponding to a simple c.t.r. with the exchange current density:

$$j_0=nFk_{\mathrm{e}}^0c_{\mathrm{ox}}^{(1-\alpha)}c_{\mathrm{red}}^{\alpha} \tag{5}$$

In Eq. 5, k_{e}^0 is the rate constant for the reaction, c_{ox} and c_{red} are the concentrations of the oxidized and reduced forms, respectively, and α is the apparent charge transfer coefficient. The exchange current per unit volume is given as:

$$j_{\mathrm{v}}=j_0S_{\mathrm{p}} \tag{6}$$

According to [10, 11], Eq. 2 expresses the charge "conservation", including the source due to the c.t.r. (or sometimes due to the partial c.t.r.). If the equilibrium polarization is taken as zero, we obtain an equation for the electrode polarization:

$$E\equiv\tilde{E}-E_{\mathrm{t}}=\phi_1-\phi_2-E_{\mathrm{t}} \tag{7}$$

At small electrode polarizations, $|E\ll R_{\mathrm{g}}T/nF$, the exponential terms in Eq. 2 can be linearized and Eq. 2 takes the following form:

$$C_1\frac{\partial\tilde{E}}{\partial t}=-\frac{1}{r_2}\frac{\partial^2\phi_2}{\partial x^2}-g_{\mathrm{ctr}}E \tag{8}$$

where $g_{\mathrm{ctr}}=AS_{\mathrm{p}}j_0\alpha nF/R_{\mathrm{g}}T$ is the charge transfer conductance per unit length. It is to be noted that $\mathrm{d}G_{\mathrm{ctr}}=g_{\mathrm{ctr}}\mathrm{d}x$ is the c.t.r. conductance of the volume element $A\mathrm{d}x$ of the electrode immersed. As has been shown [11], Eq. 8 can also be derived on the basis of the equivalent circuit with distributed elements ($\mathrm{d}R_2=r_2\mathrm{d}x$, $\mathrm{d}C=C_1\mathrm{d}x$).

In the case of low conductance of an electrode material, the resistivity per unit length of the solid phase ρ_1 is important. After averaging the potential over the volume element, ϕ_1 also becomes position dependent, i.e. $\phi_1=f(x)$. The theory of Roušar et al. [9] leads to the relation $\rho_1^{-1}\nabla^2\phi_1+\rho_2^{-1}\nabla^2\phi_2=0$, which, together with Eq. 8, gives:

$$-C_1\frac{\partial E}{\partial t}=-\frac{1}{r_1}\frac{\partial^2\phi_1}{\partial x^2}+g_{\mathrm{ctr}}E \tag{9}$$

where r_1 is the electrode material resistance per unit length. Using Eqs. 8 and 9 it is possible to obtain:

$$\frac{\partial E}{\partial t}=K\frac{\partial^2E}{\partial x^2}-kE \tag{10}$$

where the ratio of the exchange current density to the double layer capacitance determines the characteristic frequency:

$$k\equiv\frac{g_{\mathrm{ctr}}}{C_1}=\frac{j_0nF}{CR_{\mathrm{g}}T} \tag{11}$$

The so-called "field diffusion constant" K depends only on the ohmic resistivities ρ_1 and ρ_2 and on the double layer capacitance:

$$K=\frac{1}{CS_{\mathrm{e}}(\rho_1+\rho_2)} \tag{12}$$

The electrochemical impedance of an interface is determined by the potential drop E_{el} over an electrode [11]:

$$E_{\mathrm{el}}(\omega)=\phi_{1,\mathrm{a}}(d,\omega)-\phi_{2,\mathrm{a}}(0,\omega)=E_{\mathrm{a}}(d,\omega)+\phi_{2,\mathrm{a}}(d,\omega)-\phi_{2,\mathrm{a}}(0,\omega) \tag{13}$$

$$Z(\omega)=E_{\mathrm{el}}(\omega)/Aj_{\mathrm{a}} \tag{14}$$

where $\phi_{1,\mathrm{a}}(d,\omega)$ is the solid phase potential at the contact side ($x=d$), $\phi_{2,\mathrm{a}}(0,\omega)$ is the electrolyte potential at the electrolyte side ($x=0$), ω is the a.c. angular frequency, and j_{a} is the amplitude of the current density (related to the unit geometrical area of the electrode).

Using the usual electrochemistry conditions [11], the electrode impedance can be obtained as:

$$Z(\omega)=A^{-1}\left[\frac{\rho_1^2+\rho_2^2}{\rho_1+\rho_2}\frac{\coth(d\beta)}{\beta}+\frac{2\rho_1\rho_2}{\rho_1+\rho_2}\frac{1}{\beta\sinh(d\beta)}+\frac{d\rho_1\rho_2}{\rho_1+\rho_2}\right] \tag{15}$$

with:

$$\beta=\frac{1}{d}\left(\frac{k+\mathrm{i}\omega}{\omega_1}\right)^{1/2}\text{ and }\omega_1=\frac{K}{d^2} \tag{16}$$

where ω_1 is a characteristic frequency, related to the finite "field diffusion", and the parameters k and K are defined by Eqs. 11 and 12. The a.c. penetration length λ is defined as:

$$\lambda = \frac{1}{\mathrm{Re}\beta} = \left(\frac{2K/k}{(1+\omega^2/k^2)^{1/2}+1} \right)^{1/2} \quad (17)$$

If finite diffusion to the planar porous electrode takes place, then the value of the charge transfer resistance is defined as:

$$R_{\mathrm{ctr}} \rightarrow R_{\mathrm{ctr}} z(\omega) = R_{\mathrm{ctr}} \left(1 + \sqrt{\omega^2/\mathrm{i}\omega} \right) \quad (18)$$

where $z(\omega) = 1/y(\omega)$ is the value of the volume-averaged hindrance impedance, describing the deviation of a system from the conditions of the real charge transfer resistance. For a simple electrochemical c.t.r., the characteristic frequency is given as:

$$\omega_2 = k_{\mathrm{het}}^2 / D \quad (19)$$

where D denotes the diffusion coefficient of the electroactive species and $k_{\mathrm{het}} = k_{\mathrm{ox}} + k_{\mathrm{red}}$ is the rate constant. For macroscopically homogeneous surfaces, Eq. 18 seems to explain the dominant dependence that only has to be corrected for the fact that the diffusion is finite owing to the small nanopore size. The corrected hindrance impedance for a single kind of diffusing species, when the boundary condition is not a transmissive one, will be of the form:

$$z(\omega) = 1 + \sqrt{\omega_2/\mathrm{i}\omega} \coth \left(\sqrt{\mathrm{i}\omega/\omega_3} \right) \quad (20)$$

with:

$$\omega_3 = D/l_p^2 \quad (21)$$

where l_{p} denotes the characteristic pore dimension [11].

Compared with the case of a simple c.t.r., in the Paash et al. model I there are two additional parameters, ω_2 and ω_3, i.e. parameters characterizing the behaviour of the porous electrodes if finite diffusion takes place.

Experimental

The electrodes were constituted by an aluminium foil current collector and from the active material layer. The active material used consists of nanoporous carbon (prepared from TiC "stark" by a chlorination method according to the preparation scheme presented elsewhere [2, 30, 31, 32, 33, 34]), of the mixture of binder (polytetrafluoroethylene, PTFE, 60% solution in H_2O, Aldrich) and of carbon black (Aldrich). The carbon black was added to decrease the ohmic resistance of the electroactive material. This mixture was laminated on Ni foil and pressed together to form a very flexible layer of the active electrode material. After drying and plating under vacuum, this material was covered by a very pure Al layer on one side [2, 30, 31, 32, 33, 34]. After that the Al-covered carbon layer was spot-welded in an Ar atmosphere to the Al foil current collector. The limits of ideal polarizability for Al foil have been established by cyclic voltammetry as well as by impedance spectroscopy methods, and are wider than those for a carbon electrode.

The electrolytes used were prepared from very pure acetonitrile (AN; Aldrich), stored over molecular sieves before use, and from very dry Et_4NBF_4, Et_3MeNBF_4, $EtMe_3NBF_4$, $LiClO_4$ and $LiBF_4$ salts (Aldrich), additionally purified and dried [18, 30, 31, 32, 33, 34]. The three-electrode standard glass cell with a very large counter electrode (apparent area ~30 cm^2), prepared from carbon cloth, was used. The reference electrode was an aqueous saturated calomel electrode (SCE in H_2O) connected through an electrolytic salt bridge (0.1 M $LiClO_4$ in H_2O|0.1 M Et_4NBF_4 in AN) with the measurement system [18]. Very pure Ar (99.9999%, AGA) was used for saturating the solutions. Specific surface area, pore size distribution, micropore volume, micropore area and other parameters were measured using the Genimi 2375 (Micromeritic) system and calculated according to the methods described [35]. Some more important characteristics obtained are given in Table 1 and in Fig. 1. According to the data in Fig. 1, the nanopores with a pore diameter $d = 1.1$–1.2 nm prevail on the surface of carbon ID 1369. The specific area of carbon ID 1369, obtained by the Brunauer, Emmet and Teller (BET) method, has a surface area of 1100 $m^2\ g^{-1}$. Comparison of these data with those from [2] indicates that the specific surface area for ID 1369 is somewhat higher than that for nanoporous carbon ID 711.

Figure 2 demonstrates the results of AFM studies for nanoporous carbon ID 1369; according to these results, the nanoporous carbon electrode has a very rough surface.

Results and discussion

Cyclic voltammetry curves

The cyclic voltammetry (j vs. E) curves for 0.1 M electrolyte + AN solutions, obtained at small scan rates of potential $v = \mathrm{d}E/\mathrm{d}t \leq 10$ mV s^{-1}, have nearly mirror image symmetry of the current responses about the zero

Table 1 Gas phase characteristics for the electrode material prepared from nanostructured carbon ID1369

Parameter	Value
BET surface area ($m^2\ g^{-1}$)	1101
Nano(micro)pore area ($m^2\ g^{-1}$)	681
External surface area ($m^2\ g^{-1}$)	145
Micropore volume ($cm^3\ g^{-1}$)	0.28
Adsorption average pore diameter (calculated according to [35]) (Å)	27.9

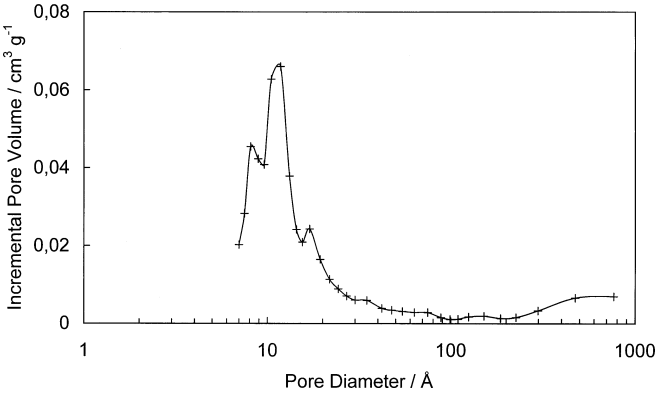

Fig. 1 Pore size distribution for nanosctructured carbon ID1369

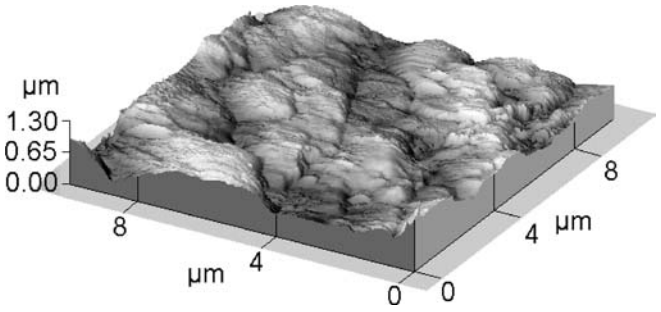

Fig. 2 Contact mode AFM images of nanostructured carbon ID1369: 10×10 μm (3D image)

current line [j = current density, obtained using the flat cross-section (geometrical) surface area]. Accordingly, the porous carbon electrodes are ideally polarizable in the region of potentials from –1.4 to 1.4 V (vs. SCE in H_2O) for Et_4NBF_4, Et_3MeNBF_4 and $EtMe_3NBF_4$ + AN solutions. For $LiClO_4$ and $LiBF_4$ + AN solutions, the region of ideal polarizability is somewhat smaller ($-1.0 < E < 1.0$ V vs. SCE), which is caused probably by the intercalation process of Li^+ cations into the nanoporous carbon or by the partial charge transfer process between Li^+ cations adsorbed on the electrode surface. The experimental data show that the shape of the j vs. E curves is independent of the number of the current cycle, n, if $n \geq 3$. Thus, the nanoporous carbon electrodes demonstrate the stable electrochemical properties in this region of potentials, i.e. in the region of ideal polarizability. At c_{el} = constant, the current responses increase almost in the expected way with large v values (Fig. 3a and b), but with increasing v (≥20 mV s^{-1}) the cyclic voltammograms become distorted from the mirror image symmetry [1]. Thus, at higher scan rates (Fig. 3c) there are very well expressed distortion effects in the j vs. E curves, caused by the significant resistivity of the electrolyte in the porous material, as well as by the high resistivity of the porous electrode material (i.e. by the significant series resistance of the experimental system). Additionally, it should be noted that the diffusion of ions (mainly cations) in the nanopores is a very slow process and thus establishment of the adsorption equilibrium is a slow process. This effect has been explained by the onset of the so-called "electrolyte starvation" effect [1, 36], which is associated with the withdrawal of the electrolyte ions from the pore bulk electrolyte owing to the adsorption of ions on the double layer interphases when they become charged. Comparison of the j vs. E curves for different electrolyte concentrations shows that the scan rate at which the deviation of the j vs. E curves from the ideal behaviour starts, decreases with the dilution of the electrolyte solution. Thus, the solution resistance is important but, on the other hand, the establishment of the adsorption equilibrium in the nanopores is a very slow process, which is caused by the very small "effective" diffusion coefficient values of the ions in the nanopores influenced by the effective diffuse layer thickness at the electrode surface, as well as

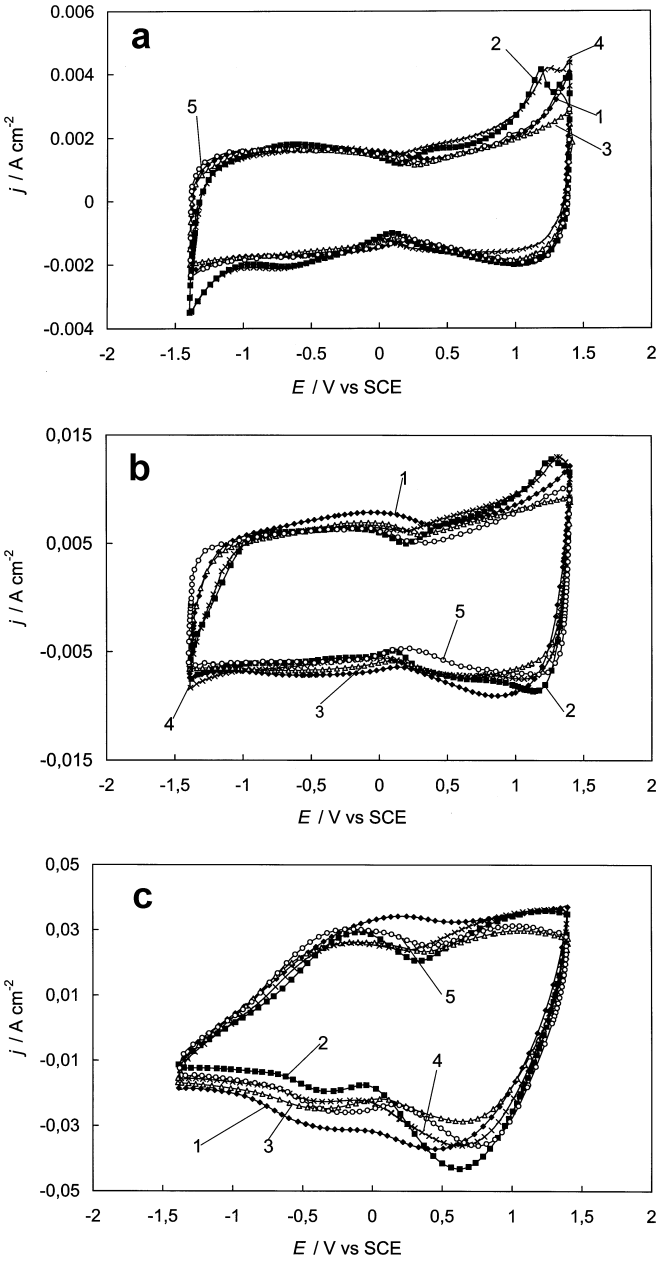

Fig. 3a–c Current density vs. potential curves for nanostructured carbon ID1369 in acetonitrile solutions with addition of 0.1 M electrolyte: Et_4NBF_4 (*1*), Et_3MeNBF_4 (*2*), $LiClO_4$ (*3*), $LiBF_4$ (*4*) and $EtMe_3NBF_4$ (*5*) at potential scan rates v (mV s^{-1}): 2 (**a**); 10 (**b**); and 50 (**c**)

by the increase of the effective Debye screening length with the dilution of the electrolyte [1, 2, 18, 34, 36, 37, 38, 39, 40].

Figure 3a and b shows that, in the j vs. E curves obtained at small scan rates, there is a minimum of current density in the region of potentials $-0.1 \leq E \leq 0.5$ V (vs. SCE in H_2O), which, in the case of metal electrodes, is explained by the diffuse nature of the electric double layer in the region of total (or free) zero charge [18]. Noticeably better expressed current minima have been established for the 0.01 M and 0.005 M

Et_4NBF_4 + AN solutions [2], and the current density at v = constant and $E = E_{min}$ decreases with dilution of the electrolyte. Thus, this minimum is probably caused by the zero charge potential (or by the total zero charge potential) of the porous carbon electrode [1, 2, 15, 16, 17, 18]. The potential of this minimum is practically independent of the direction of the potential scan if $v \leq 2$ mV s^{-1}, as well as of the electrolyte concentration if $c_{el} \leq 0.1$ M.

Differential capacitance vs. potential curves

The values of the differential capacitance, corresponding mainly to the double layer capacitance, can be obtained as:

$$C = jv^{-1} = j(dE/dt)^{-1} \tag{22}$$

if we assume that the capacitance C = constant and if the system series resistance $R \rightarrow 0$ or if the current $I \rightarrow 0$. If $R \neq 0$ and $I \neq 0$, for cyclic voltammetry the applied voltage E_t is given as:

$$E_t = E_0 + vt - IR \quad (\text{for } 0 \leq t \leq E_2/v) \tag{23}$$

where E_0 is the initial potential, t is time, R is resistance, and E_2 is the upper limit of the potential sweep. Correspondingly, the voltage applied during the negative direction of the potential sweep is:

$$E_t = E_2 - vt - IR \tag{24}$$

Assuming that R = constant and $I = f(t)$, the following expressions for the positive (anodic) current:

$$I_a(E) = Cv - RC\frac{dI}{dt} \tag{25}$$

and for the negative (cathodic) current:

$$I_c(E) = -Cv - RC\frac{dI}{dt} \quad \text{for } E_2/v \leq t \leq 2E_2/v \tag{26}$$

can be obtained. Thus, Eq. 22 can be used for obtaining the capacitance values only in the region of small potential scan rates if the values of the current are very small, as the potential drop (IR drop) losses are negligible only at these conditions, and the current response is essentially that of a pure capacitor [5].

The C vs. E curves in Fig. 4a–c, obtained from j vs. E curves, show that at $E \approx 0.30$ V (vs. SCE in H_2O) the very well expressed capacitance minimum (with the potential of the minimum E_{min}) in C vs. E curves has been observed. According to the data in Fig. 4a, for 0.1 M Et_4NBF_4 + AN solution in the limited region of the electrode potential, corresponding to the zero charge potential $E_{\sigma=0} = 0.30$ V (vs. SCE in H_2O), the capacitance is practically independent of v. The same is valid for other electrolytes consisting of tetraalkylammonium cations. It should be noted that the values of C established from j vs. E curves at $v \leq 5$ mV s^{-1} are in good agreement with the C_s vs. E curves (Fig. 5a–e) [where C_s is the series capacitance, calculated from the complex plane (Z'' vs. Z') plots], measured at an a.c. frequency $f \leq 10$ mHz. According to the experimental data, the series differential capacitance is independent of f only at $f \leq 0.01$ Hz, demonstrating that the almost equilibrium capacitance values (given in Table 2) have been established in the region of zero charge potential. At higher frequency, C_s depends significantly on f, which is caused by the very small values of the a.c. penetration depth (Eq. 17) compared with the pore length. The potential of

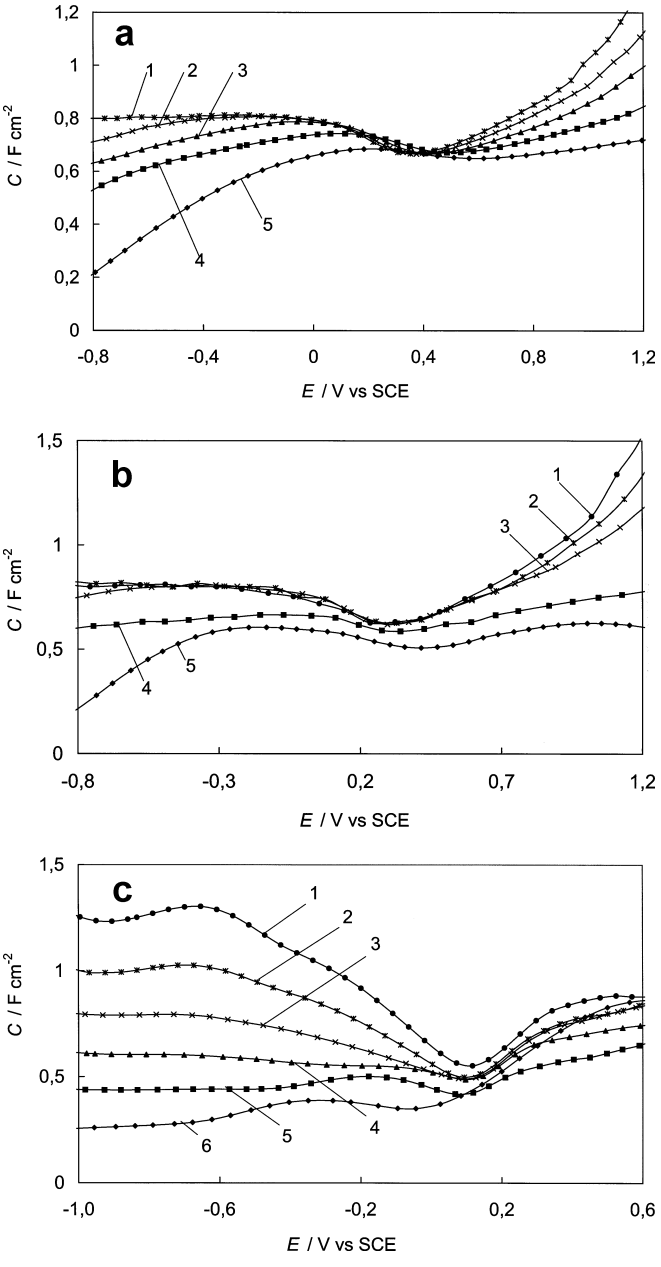

Fig. 4a–c C vs. E curves for nanostructured carbon ID1369 in acetonitrile solutions with addition of 0.1 M electrolyte: **a** Et_4NBF_4, **b** Et_3MeNBF_4 and **c** $LiBF_4$, obtained from j vs. E curves at potential scan rates v (mV s^{-1}): **a** 2 (*1*), 5 (*2*), 10 (*3*), 20 (*4*) and 50 (*5*); **b** 1 (*1*), 2 (*2*), 5 (*3*), 20 (*4*) and 50 (*5*); **c** 2 (*1*), 2 (*2*), 5 (*3*), 10 (*4*), 20 (*5*) and 50 (*6*) (**a**, **b**: positive direction of potential scan; **c**: negative direction of potential scan)

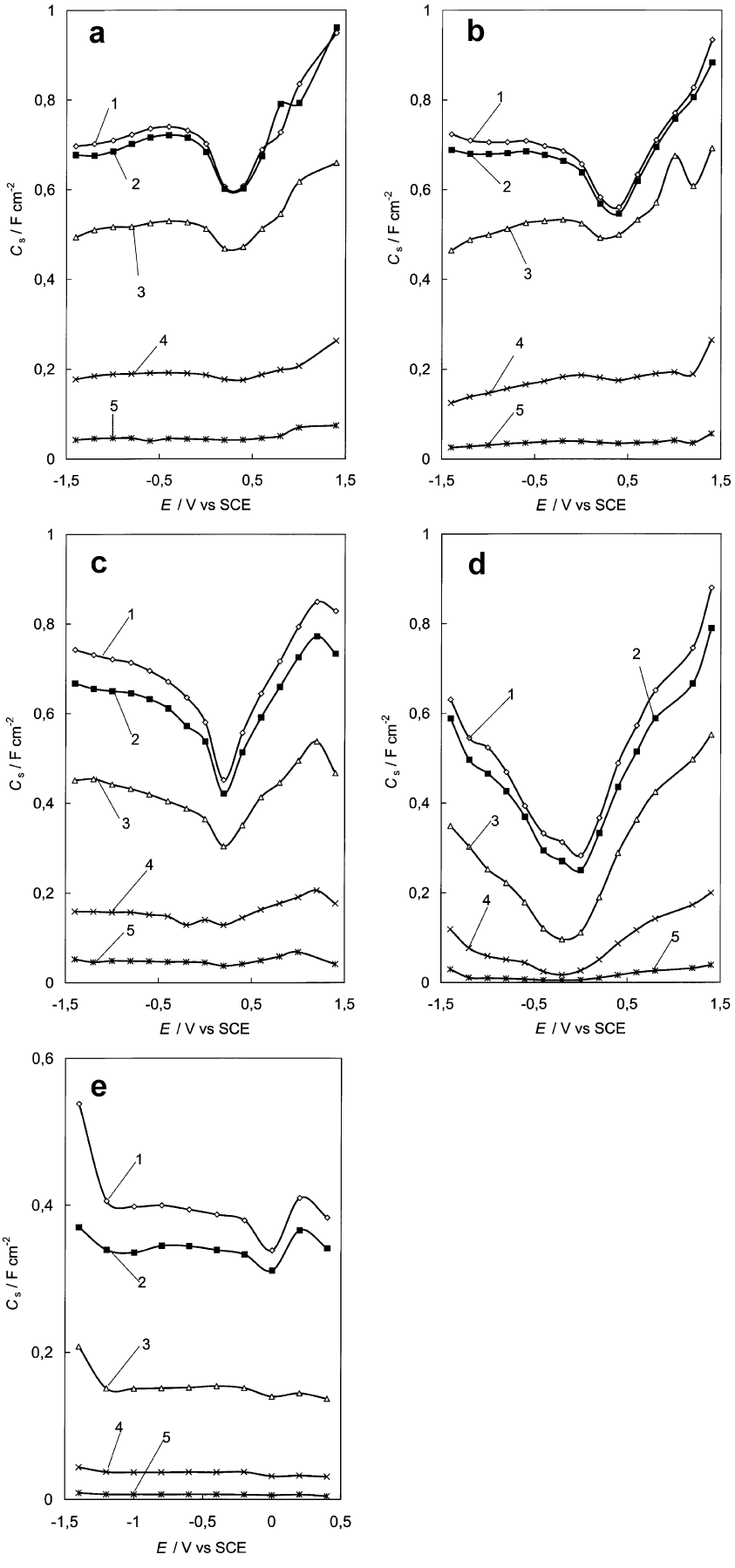

Fig. 5a–e C_s vs. E curves for nanostructured carbon ID1369 in acetonitrile solutions with addition of 0.1 M electrolyte: **a** Et_4NBF_4, **b** Et_3MeNBF_4, **c** $EtMe_3NBF_4$, **d** $LiBF_4$ and **e** $LiClO_4$, obtained from $-Z''$ vs. Z' curves at different a.c. frequencies f (Hz): 0.005 (*1*), 0.01 (*2*), 0.1 (*3*), 1.0 (*4*) and 10 (*5*)

Table 2 Electrochemical characteristics of nanoporous carbon ID 1369 in acetonitrile solutions of various electrolytes[a]

Electrolyte	$E_{\sigma=0}$ (V vs. SCE)	$C_{s,min}$ (F cm^{-2}) (f = 5 mHz)	f_{max} (Hz)	α
Et_4NBF_4	0.30	0.60	31620	0.96
Et_3MeNBF_4	0.35	0.56	5010	0.97
$EtMe_3NBF_4$	0.20	0.45	4560	0.88
$LiBF_4$	0.01	0.28	31620	0.86
$LiClO_4$	0.00	0.34	7940	0.66

[a] $E_{\sigma=0}$ = zero charge potential; $C_{s,min}$ = series differential capacitance at $E_{\sigma=0}$; f_{max} = characteristic frequency; α = fractional exponent

the capacitance minimum in C_s vs. E curves is independent of frequency if $f \leq 0.01$ Hz. At $|E| > E_{\sigma=0}$, there is a noticeable dependence of C_s on f as well as of C_{min} on v (Fig. 6), which is caused by the very small values of the diffusion coefficients of the anions in the pores, as well as by the essential IR drop at $v > 10$ mV s^{-1} and at E far from $E_{\sigma=0}$.

According to the data in Fig. 6, for Et_4NBF_4, Et_3MeNBF_4 and $EtMe_3NBF_4$, the dependence of C_{min} on the potential scan rate is small at $v^{1/2} \leq 3$ mV$^{1/2}$ s$^{-1/2}$ and, thus, the equilibrium values of the differential capacitance have been obtained. The comparison of the capacitance values demonstrates that C_{min} increases in the order $LiBF_4 < LiClO_4 \leq EtMe_3NBF_4 < Et_3MeNBF_4 < Et_4NBF_4$ (Table 2), i.e. with the increase of molar mass of the electrolyte. At $v^{1/2} \geq 3.5$ mV$^{1/2}$ s$^{-1/2}$, there is a linear dependence of C on $v^{1/2}$, as well as on $\omega^{1/2}$ (if $f \geq 0.01$ Hz), characteristic of the diffusion-limited process. For the electrolytes containing Li^+ ions, at $v^{1/2} \leq 0.7$ mV$^{1/2}$ s$^{-1/2}$, a very large dependence of C on $v^{1/2}$ has been established, indicating that the charge transfer (or partial charge transfer) process is possible between the surface of the carbon electrode and the Li^+ ions adsorbed.

At higher scan rates, the value of E_{min}, obtained from j vs. E curves, depends on the direction of the potential scan (Fig. 7), which is caused by the influence of the IR drop (Eqs. 23, 24, 25, 26), as well as by the very slow processes of adsorption-desorption (with partial charge transfer) and diffusion of ions in the nanopores. With the decrease of v lower than 5 mV s^{-1}, the difference between the E_{min} values for positive- and negative-going potential scans decreases (Fig. 7) and the E_{min} value, corresponding to zero charge potential of the nanoporous carbon electrode, obtained by the extrapolation of E_{min} vs. v dependence on the condition $v = 0$, can be established. These values of E_{min} are in good agreement with the $E_{\sigma=0}$ values obtained from C_s vs. E curves. However, it should be noted that for more detailed analysis of the physical nature of the minimum in the C_s vs. E curves, future experimental investigations in more dilute electrolyte solutions, as well as in conditions $v \leq 0.5$ mV s^{-1}, are inevitable.

It should be noted that the dependence of E_{min} on v is smallest for $EtMe_3NBF_4$, and this dependence increases in the order $EtMe_3NBF_4 < Et_3MeNBF_4 < Et_4NBF_4$, i.e. with the increase of surface activity of the cation (higher capacitance values at E_{min}) with the molar mass of the ions. The value of $E_{\sigma=0}$ (given in Table 2) depends on the geometrical structure and chemical nature of the cations, and $E_{\sigma=0}$ shifts toward more positive values with the increase of molar mass of the cations, i.e. in the order of the electrolytes $LiClO_4 < LiBF_4 < EtMe_3NBF_4 < Et_4NBF_4 < Et_3MeNBF_4$ (Table 2). The somewhat less positive $E_{\sigma=0}$ value for $LiClO_4$, compared with that for $LiBF_4$, is caused mainly by the higher surface activity of ClO_4^- anions compared with BF_4^-; as for $LiClO_4$ solutions [18], the values of C_{min} and C_s at $E_{\sigma=0}$ are higher.

Analysis of impedance data

The $-Z''$ vs. Z' plots [so-called Nyquist plots (Fig. 8)] were measured for nanoporous carbon ID 1369|0.1 M

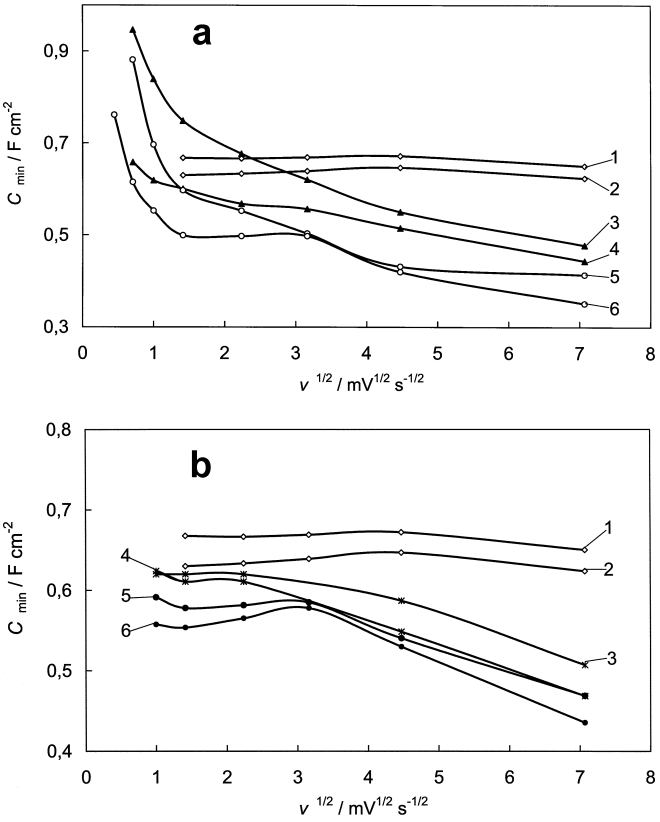

Fig. 6a,b C_{min} vs. $v^{1/2}$ curves for nanostructured carbon ID1369 in acetonitrile solutions with addition of 0.1 M electrolyte: **a** Et_4NBF_4 (*1*, *2*), $LiClO_4$ (*3*, *4*) and $LiBF_4$ (*5*, *6*); **b** Et_4NBF_4 (*1*, *2*), Et_3MeNBF_4 (*3*, *4*) and $EtMe_3NBF_4$ (*5*, *6*), obtained from j vs. E curves for positive (*1*, *3*, *5*) and negative (*2*, *4*, *6*) directions of the potential scan

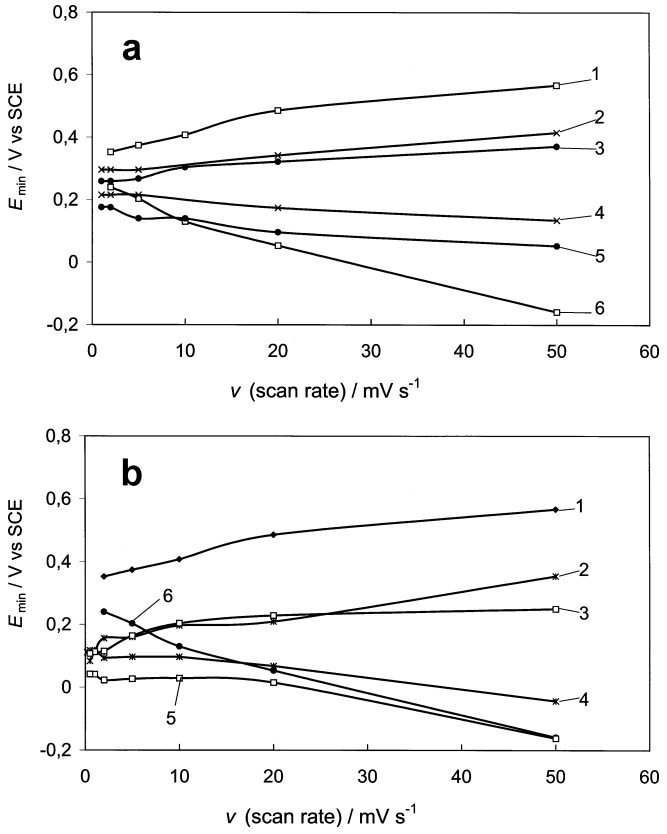

Fig. 7a,b E_{min} vs. potential scan rate (v) curves for nanostructured carbon ID1369 in acetonitrile solutions with addition of 0.1 M electrolyte: **a** Et_4NBF_4 (*1*, *6*), Et_3MeNBF_4 (*2*, *4*) and $EtMe_3NBF_4$ (*3*, *5*); **b** Et_4NBF_4 (*1*, *6*), $LiBF_4$ (*2*, *4*) and $LiClO_4$ (*3*, *5*), obtained from j vs. E curves for positive (*1*, *2*, *3*) and negative (*4*, *5*, *6*) directions of the potential scan

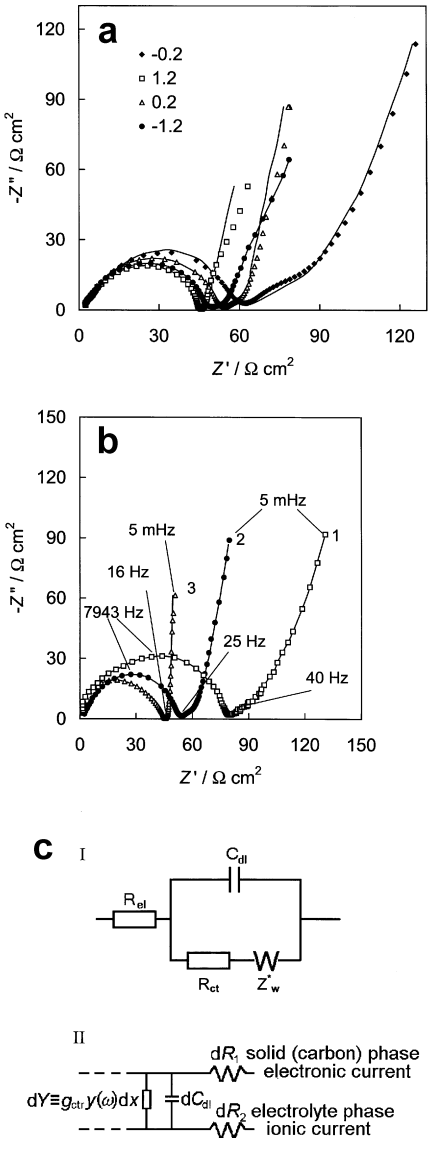

Fig. 8a–c Complex plane ($-Z''$ vs. Z') plots for a nanostructured carbon ID1369|acetonitrile + 0.1 M $LiBF_4$ interface at different electrode potentials, noted in **a**, and at **b** $E = 0.2$ V (SCE) for 0.1 M $LiClO_4$ (*1*), $LiBF_4$ (*2*) and Et_3MeNBF_4 (*3*). Symbols: experimental data, *solid lines*: simulation according to Meyer et al. model [48] [**a** and **b** (*1*, *2*)] and according to Paasch et al. model I (*3*). **c** Equivalent circuits: *I*: Ho et al. model [46] (where R_{el} is the electrolyte solution resistance, C_{dl} is the double layer capacitance, R_{ct} is the charge transfer or adsorption or partial charge transfer resistance and Z_w is the generalized finite length Warburg element for a short-circuit terminus model [40, 45]); *II*: Paasch et al. model I [11] {where dY is the complex admittance of the hindered c.t.r. [involving the hindrance factor $y(\omega)$ of the c.t.r. with the charge transfer conductance g_{ct}]; dC_{dl} is the double layer capacitance; dR_1 and dR_2 are the ohmic resistance of the porous electrode material and of the electrolyte in the pore, respectively, in the volume element $A dx$}

electrolyte + AN solutions in the range of a.c. frequencies from 1×10^{-3} to 1×10^{5} Hz and in the region of potentials from –1.4 to 1.4 V (vs. SCE in H_2O) at fixed E = constant. The solid lines in Fig. 8a and b have been simulated according to the Ho et al. circuit I [46], Paasch et al. circuit II [11] or Meyer et al. model [48] (more detailed analysis will be given later). The experimental results obtained demonstrate that the shape of the $-Z''$ vs. Z' plots depends noticeably on E (Fig. 8a) as well as somewhat on the electrolyte composition (Fig. 8b). The complex plane plot for Et_4NBF_4, Et_3MeNBF_4 or $EtMe_3NBF_4$ + AN electrolyte consists mainly of two parts: the depressed semicircle at higher a.c. frequencies ($f \geq 40$ Hz) with the characteristic frequency f_{max} (given in Table 2) and the so-called double layer capacitance region at lower frequencies (so called "planar electrode" section where finite length effects prevail). The shape of the $-Z''$ vs. Z' plots indicates that there are two limiting processes (the slow diffusion and slow heterogeneous adsorption steps, with the faradaic charge transfer or partial charge transfer process) affecting the rate of the adsorption of the electrolytes at the nanoporous carbon|AN interface at $f > 40$ Hz [1, 2, 28, 40, 41, 42, 43, 44, 45, 46, 47, 48, 49]. Differently from the nanoporous carbon ID 711|AN + 0.1 M Et_4NBF_4 interface [2] and from ID 1369|0.1 M $LiClO_4$ or 0.1 M $LiBF_4$ + AN systems (Fig. 8a), there is not a very well expressed so-called nanoporous region in the $-Z''$ vs. Z' plots (i.e. there is no section in the $-Z''$ vs. Z' plots where the slope

$\alpha' = 45°$, characteristic of a diffusion-limited process in the nanopores [1, 2, 36, 45, 46, 47, 48, 49]). It should be noted that the so-called "pore resistance" depends on the surface charge density and is a maximum in the region of zero charge density (Fig. 8a). Thus, the "pore resistance" depends on the effective screening length of the ions in the electrical double layer [39]. Only in the region of zero charge potential is there a very compressed region, where the $-Z''$ vs. Z' plots for Et_4NBF_4, Et_3MeNBF_4, and $EtMe_3NBF_4$ are almost linear with a slope $\alpha' \approx 45°$. For that reason, it is impossible to obtain correctly the electrochemical parameters of the pores prevailing at the surface of the nanoporous carbon ID 1369 material. The dependence of the slope of the $-Z''$ vs. Z' plot on the electrode potential in the so-called planar electrode section ($f < 20$ Hz) is caused mainly by the decrease of the effective screening length of the electrolyte ions with the increase of the surface charge density at the electrode|electrolyte interface [39, 50]. It should be noted that the effective diffuse layer thickness (i.e. the inverse Debye length of the electrolyte ions) as a function of the electrode rational potential $E = E_x - E_{\sigma=0}$ is given as $\kappa_{eff}(E) = \kappa \cos(e\beta E/2)$, where κ is the Gouy length. The Debye length (equal to κ^{-1}) is obtained as $\kappa^{-1} = \left(\varepsilon\beta/8\pi n e^2\right)^{1/2}$, where $\beta = (k_B T)^{-1}$ (T is the absolute temperature and k_B is the Boltzmann constant; n is the bulk electrolyte concentration; ϵ is the dielectric constant of the solvent; and e is the elementary charge). The crystallographic ion radius (r_{CR}) increases in the order of the cations as $Li^+ < EtMe_3N^+ < Et_3MeN^+ < Et_4N^+$, but the radii of the BF_4^- and ClO_4^- anions are practically the same [37, 38]. According to the experimental data for Et_4NBF_4 in various solvents, the Walden product $\left(\eta^0 \lambda^0_{Et_4N^+}\right)$ is practically independent of the solvent studied, and therefore the radius of this tetraethylammonium ion in AN solution, to a first approximation, can be taken as equal to the crystallographic radius of this cation ($r_{CR} = 0.343 \pm 0.002$ nm) [37, 38] (η^0 is the coefficient of viscosity for the pure solvent; λ^0 is the limiting molar conductivity of AN with addition of Et_4NBF_4). Thus, the dependence of the shape of the $-Z''$ vs. Z' plot on E indicates that the effective pore dimension is of the same order of magnitude as the Debye length for the 0.1 M electrolyte + AN system ($\kappa^{-1} = 0.66$ nm for 0.1 M electrolyte in AN at $T = 298$ K and $E = E_{\sigma=0}$).

The $-Z''$ vs. Z' plots (at $f =$ constant) were used for the calculation of the values of the differential series capacitance C_s (series circuit) and parallel capacitance C_p (parallel circuit), as well as of the series resistance R_s and parallel resistance R_p values (Fig. 9). According to the data obtained, the C_s and C_p values level off to the limiting value of $C_s(\omega \to 0)$ at very low frequency, $f \leq 0.01$ Hz, indicating that diffusion is a very slow and limiting stage of the adsorption process of the tetraalkylammonium ions in the region of zero charge potential as well as at $E << E_{\sigma=0}$. Comparison of the C_s values obtained from impedance data with the values of C obtained from j vs. E curves demonstrates a good agreement between the differential capacitance values of both series at $E \leq E_{\sigma=0}$ if $f \leq 10^{-2}$ Hz and $v \leq 1$ mV s^{-1}.

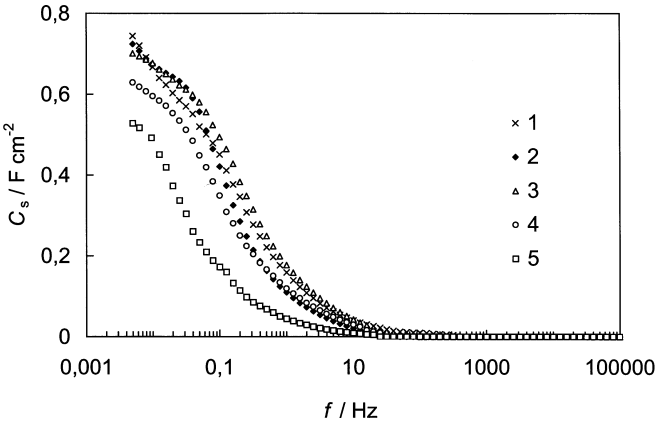

Fig. 9 C_s vs. f curves for nanostructured carbon ID1369 in acetonitrile solutions with addition of 0.1 M electrolyte: $EtMe_3NBF_4$ (*1*), Et_3MeNBF_4 (*2*), Et_4NBF_4 (*3*), $LiBF_4$ (*4*) and $LiClO_4$ (*5*) at $E = -1.4$ V vs. SCE

At $c_{el} =$ constant, the values of $C_s(\omega \to 0)$ are somewhat higher for the positively charged surfaces than those at $E < E_{\sigma=0}$, indicating that the Gibbs adsorption for cations is lower than that for anions. The inflection frequency for C_s vs. f and C_p vs. f plots depends on the electrolyte studied, and the value of f decreases with molar mass of the tetraalkylammonium cation studied. At $E > 1.0$ V (vs. SCE), the values of $C_s(\omega \to 0)$ are higher than the values of $C_p(\omega \to 0)$, indicating that the faradaic process or the partial charge transfer process is possible [1, 2, 28, 40, 41, 42, 43] at the nanoporous carbon|electrolyte interface if the weak specific adsorption of BF_4^- or ClO_4^- anions takes place on nanoporous carbon.

Figure 10 demonstrates the Bode amplitude ($|Z|$ vs. $\log\omega$) plots for various electrolytes obtained at different electrode potentials, $E =$ constant. According to these data, the shape of the $|Z|$ vs. $\log\omega$ plots depends on the

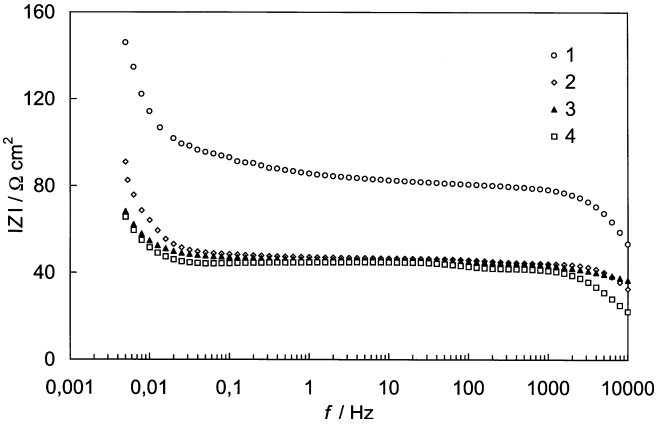

Fig. 10 $|Z|$ vs. f curves for nanostructured carbon ID1369 in acetonitrile solutions with addition of 0.1 M electrolyte: $LiClO_4$ (*1*), $LiBF_4$ (*2*), Et_4NBF_4 (*3*) and Et_3MeNBF_4 (*4*) at $E = -1.4$ V vs. SCE

electrolyte composition as well as on the electrode polarization. The higher values of $|Z|$ for the 0.1 M $LiClO_4$ solution are caused mainly by the higher resistance of the faradaic reaction as well as by the higher values of the pore resistance (Fig. 8a and b). At $1\times10^{-1} \le f \le 1\times10^{3}$ Hz, there is no dependence of $|Z|$ on the electrode potential and frequency. At $f \ge 0.1$ Hz the $|Z|$ vs. logω plots have a slope of ca. –45°, which is characteristic of the kinetically mixed process, i.e. of the process limited by the slow diffusion and charge transfer (or partial charge transfer in our case) stages [simulated by the equivalent circuit where the Warburg diffusion impedance and the charge transfer resistance are connected in series in the equivalent circuit (Fig. 8c)] [1, 2, 40, 41, 42, 43]. The dependence of the phase angle δ on logω is in very good agreement with the data in Fig. 10, and the values of δ are systematically lower in the potential region $E > E_{\sigma=0}$ than at $E < E_{\sigma=0}$.

Analysis of complex plane plots

The complex plane plots, measured and simulated for the nanoporous carbon ID 1369|0.1 M AN + 0.1 M $LiClO_4$ (or $LiBF_4$) interface at E = constant (Figs. 8a and b and 11a and b), can be divided into four main sections. At high a.c. penetrability (at very low a.c. frequency $f \le 1\times10^{-2}$ Hz and at very high values of λ) the nanoporous carbon electrode behaves like a planar electrode since the penetration depth λ (Eq. 17) is larger than the length of a pore so that an a.c. signal detects a very large amount of the pore volume. However, according to the data in Figs. 8 and 11, in this region of f, the nanoporous carbon|AN interface demonstrates non-ideal constant phase element (CPE) behaviour and constant phase exponent values of α less than 1.0 have been established: $\alpha \approx 0.97$ for Et_3MeNBF_4 and α decreases in the order of the electrolytes as $Et_3MeNBF_4 > Et_4NBF_4 > EtMe_3NBF_4 > LiBF_4 > LiClO_4$ (Table 2). The values of α depend on the electrode potential (as well as on the electrolyte concentration), indicating that the specific adsorption of ions at different values of E (cations at $E < E_{\sigma=0}$ and anions at $E > E_{\sigma=0}$) is possible [40, 43]. On the other hand, at c_{el} = const, the dependence of α on $|E|$ indicates that the effective working surface area of the electrode depends on the surface charge density [2, 39, 44, 45, 50]. Additionally, it should be noted that the decrease of α with positive polarization for $LiClO_4$ and $LiBF_4$ salts at c_{el} = constant can be explained by the increasing influence of the faradaic processes with the increase of electrode polarization or by the partial charge transfer process at $E >> E_{\sigma=0}$ [40, 43, 45, 46].

However, according to the model developed in [49], the deviation of α from unity is caused mainly by the pore size distribution in the nanoporous material studied. With the dilution of the electrolyte, the effective diameter of the ions solvated increases and the porous electrode seems more flat and less porous [2, 37, 38, 39, 44]. It should be noted that more detailed computer simulations are inevitable, but the somewhat higher deviation of α from unity for ID 1369, compared with ID 711 [2], indicates that the nanoporous carbon ID 711 has a narrow pore size distribution, which is in good agreement with the BET data (Table 1 and Fig. 1 and the corresponding data in [2]).

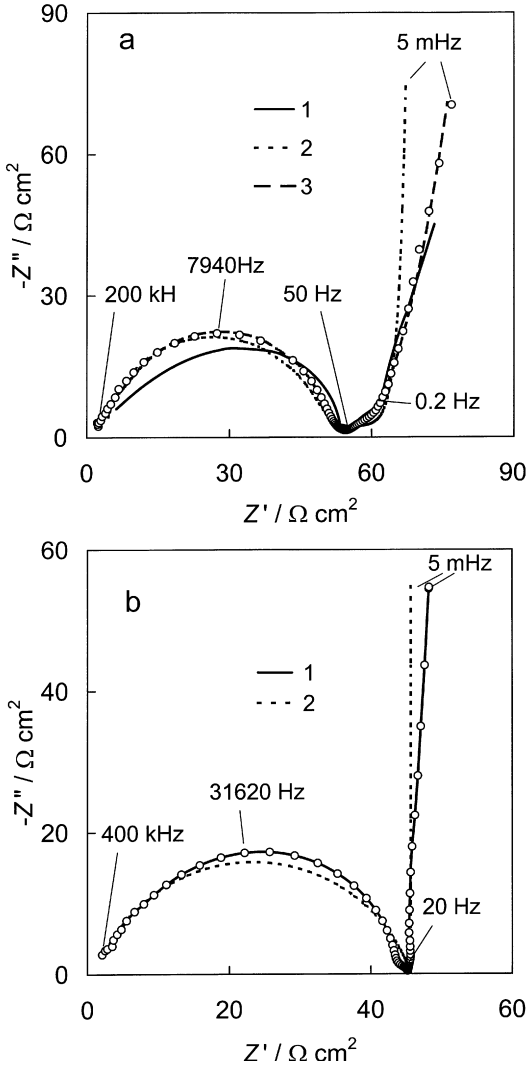

Fig. 11a,b Complex plane plots for nanostructured carbon ID1369 in acetonitrile solutions with addition of 0.1 M electrolyte: **a** $LiBF_4$ and **b** Et_4NBF_4 at the electrode potential E = 0.2 V vs. SCE. *Marks*: experimental data, *solid lines*: data calculated according to the Paasch et al. model I [11] (*1*); Ho et al. model [46] (*2*); and Meyer et al. model [48] (*3*) (see legend of Fig. 8c)

At lower penetrability (at higher frequency), the penetration depth is smaller than the length of the pores, so the a.c. signal detects only a part of the pore volume, i.e. of the nanopore surface. This is called the porous section of the $-Z''$ vs. Z' plots, and the phase angle approaches –45° in this region of the a.c. frequency (Figs. 8 and 11). In addition, there is a transition section between the porous and the planar sections in the $-Z''$ vs. Z' plots.

At higher frequencies there is a very well expressed, slightly depressed, semicircle in the $-Z''$ vs. Z' plots, with the depression angle β decreasing in the order $EtMe_3NBF_4 \geq Et_3MeNBF_4 \geq LiBF_4 \geq LiClO_4 \geq Et_4NBF_4$. It should be noted that the value of β equal to zero corresponds to the purely charge transfer limited heterogeneous process, $\beta = 45°$ corresponds to the diffusion limited stage, and $0 < \beta < 45°$ (depressed semicircle) corresponds to a charge transfer process at the inhomogeneous interfaces [2, 40, 41, 42, 43, 44, 45, 46, 47]. The value of $\beta \approx 0$ for the $Et_4NBF_4 + AN|ID\ 1369$ interface indicates that the very fast heterogeneous adsorption step (i.e. the partial c.t.r.) is probably the rate-determining process for this system at $f \geq 40$ Hz. For the ID 1369$|EtMe_3NBF_4$ and ID 1369$|Et_3MeNBF_4$ interfaces, the diffusion-limited process has been established, i.e. adsorption is limited mainly by the diffusion step ($\beta \approx 45°$ for $EtMe_3NBF_4$ and $\beta \approx 40°$ for Et_3MeNBF_4).

Results of non-linear regression analysis of the $-Z''$ vs. Z' plots in the region of higher frequencies ($f > 40$ Hz) show that these plots can be simulated using the Ho et al. (i.e. modified Randles-like) equivalent circuit [inset in Fig. 8c (scheme I)], where the generalized finite length Warburg element (GFW) for a short-circuit terminus model is expressed as [40, 45]:

$$Z_{GFW} = \frac{R_D \tanh[(iT\omega)^{\alpha_W}]}{(iT\omega)^{\alpha_W}} \tag{27}$$

where R_D is the so-called limiting diffusion resistance, the parameter T is expressed as $T = L^2/D$, where L is the effective diffusion layer thickness and D is the effective diffusion coefficient of a particle, and α_W is a fractional exponent varying from 0 to 1. The parallel charge transfer or adsorption resistance, R_{ct} (Fig. 12a), depends on the electrode potential, indicating that the deviation of our system from the ideally polarizable electrode with a smooth surface increases in the order of the electrolytes as $Et_3MeNBF_4 < Et_4NBF_4 < EtMe_3NBF_4 < LiBF_4 < LiClO_4$. According to the data in Fig. 12b–d, the values of R_D, T and α_W depend on E as well as on the electrolyte, indicating that the structure of the adsorption layer depends on the surface charge density as well as on the geometrical structure of the ions adsorbed.

According to the data in Figs. 8a and 11a, the adsorption kinetics of $LiBF_4$ and $LiClO_4$ at the ID 1369 surface is limited by two rate-determining processes, i.e. probably by the slow diffusion and heterogeneous adsorption steps, followed by the true faradaic process, i.e. by the intercalation of Li^+ ions into the carbon phase at

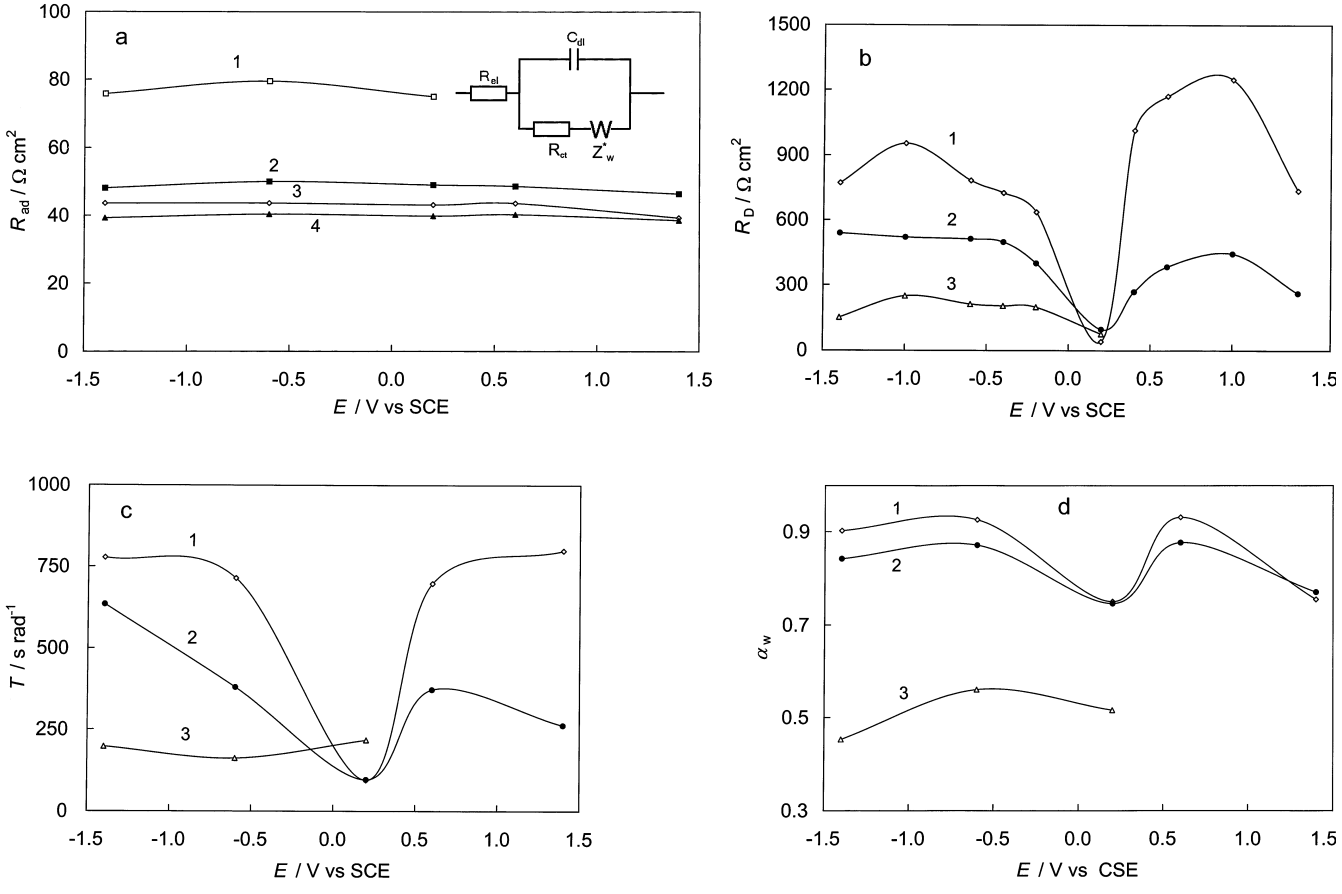

Fig. 12a–d The dependences of the parameters **a** R_{ad}, **b** R_D, **c** T and **d** α_W on the electrode potential (calculated according to modified Randles-like model) for nanostructured carbon ID1369 in acetonitrile solutions with addition of 0.1 M electrolyte: **a** $LiClO_4$ (*1*), $LiBF_4$ (*2*), Et_4NBF_4 (*3*) and Et_3MeNBF_4 (*4*); and **b, c, d** Et_3MeNBF_4 (*1*), Et_4NBF_4 (*2*) and $LiClO_4$ (*3*). Inset of the part **a**: modified Randles-like equivalent circuit (i.e. Ho et al. model) (see legend of Fig. 8c)

$E < E_{\sigma=0}$. Thus, for the carbon|Li^+ + AN interface at a frequency $f > 40$ Hz, to a first approximation the Ho et al. model seems to be valid [46] and the insertion reaction of Li^+ cations into the thin surface film of the electrode is possible. However, differently from the experimental data in Figs. 8a and 11a, this model predicts that at low ω the values of Z' are practically independent of ω and, thus, $-Z''$ vs. Z' plots have to be linear lines parallel to the Z'' axis at $f \to 0$. A better agreement between the theoretical simulations and experimental results can be established using the Bisquert et al. model [47], where the constant phase element (CPE) for the simulation of the capacitance (impedance) values at very low frequencies has been used, i.e. the finite length diffusion model with the reflective boundary conditions has been introduced. However, a better agreement between simulations and experimental data for a nanoporous carbon|$LiClO_4$ + AN (or $LiBF_4$ + AN) interface has been established if the Meyer et al. model [48] is used, in which the charge transfer and double layer charging at the surface, the solid phase diffusion inside the nanoparticle (i.e. in the nanoporous material) and the dependence of the open-circuit potential on the intercalant concentration, as well as the effect of an insulating film at the nanoporous surface (or surrounding the nanoporous particle), have been taken into account. The results in Figs. 8a and b and 11b show that the theoretical fit of the experimental data is excellent at $E < E_{\sigma=0}$. However, for positively charged surfaces there are deviations at lower frequencies and, at these potentials, a better fit would be established if the Paasch et al. model I [11] is used. For ID 1369|0.1 M tetraalkylammonium cation + AN systems (Figs. 8b and 11b), in the whole potential region a better fit has been established by Paasch et al. model I [11]. According to the results of non-linear regression analysis [11, 45], the chi-squared function (χ^2) has the usual values ($\chi^2 \leq 1\times10^{-2}$) for the electrochemistry when the complicated materials and systems are studied. The error values of individual parameters are comparatively small, and the data in Figs. 8b, 11b and 13 indicate that this model can be used for the simulation of the $-Z''$ vs. Z' plots for Et_4NBF_4, Et_3MeNBF_4 or $EtMe_3NBF_4$ + AN|ID1369 interfaces and, accordingly, the polarization propagates like diffusion (parameter $\omega_0 = k\sqrt{3}$) through the electrode of finite thickness (related to ω_1), and that at any point, x, the finite diffusion, related to ω_2 and ω_3, results in a further time delay. Thus, the two parallel conduction paths in the solid and liquid phases are interconnected by the double layer capacitance in parallel with the complex admittance of the hindered c.t.r. (the equivalent circuit II in the inset of Fig. 8c).

Additionally, the Paasch et al. model II [11, 45] was used where the polarization field $E(\kappa,\omega)$, responsible for the c.t.r., is not restricted to the volume average of the polarization of the interface, but can be extended into the solid phase [19]. The results of the non-linear regression analysis demonstrate the noticeably higher deviation of calculated $-Z''$ vs. Z' curves from the experimental data for this model than that for the Paasch et al. model I [11], and therefore these data will not be discussed in more detail in this paper.

The dependencies of the characteristic frequencies ω_1 and ω_3 and of the function $y = d\left(\rho_1^2 + \rho_2^2\right)/(\rho_1 + \rho_2)$ on the electrode potential (calculated according to the Paasch et al. model I [11]) are given in Fig. 13. According to our simulations, the values of ω_2, $\omega_3 << \omega_0$, and then the relative magnitudes of ω_1, ω_2 and ω_3 determine the low-frequency behaviour of the $-Z''$ vs. Z' plots. At very low frequency, $f \leq 5\times10^{-2}$ Hz, there is a transition to pure capacitive behaviour, since both the field diffusion and the species diffusion are finite. In the region of frequencies $0.2 < f < 10$ Hz, the absolute value of the slope equal to $\pi/4$ for the $-Z''$ vs. Z' plots was observed around ω_2, where the diffusion of species dominates in the solution phase. Figure 13b indicates that the characteristic frequency k, determined by the ratio of the exchange current density j_0 to the double layer capacitance $[k \equiv \omega_0/\sqrt{3} = j_0 nF/(CR_gT)]$, increases in the order of electrolytes as $EtMe_3NBF_4 < Et_3MeNBF_4 < Et_4NBF_4$. Thus, j_0 increases in the order of the electrolytes given above as the double layer capacitance only depends a very little on the electrolyte studied. The field diffusion constant $K = \omega_1 d^2$ (obtained from Fig. 13c) increases in the order $LiBF_4 < EtMe_3NBF_4 < Et_3MeNBF_4 < LiClO_4 < Et_4NBF_4$ if we accept that the electrode thickness d = constant. The dependence of the function y on E as well as on the electrolyte type indicates that the value of ρ_2 (the electrolyte resistance per unit length) depends very noticeably on the electrolyte as well as on the electrode polarization, because the value of d (thickness of the electrode material) and ρ_1 (the electrode material resistance per unit length) have to be independent of the electrolyte studied. For nanoporous carbon ID 1369|0.1 M Et_4NBF_4, Et_3MeNBF_4 or $EtMe_3NBF_4$ + AN interface at higher frequency ($f \geq 40$ Hz), the shape of the impedance spectra is determined mainly by the ratio of the ω_0 and ω_1 values, i.e. without regard to diffusion in the pores [11].

Conclusions

The results of impedance studies at nanoporous carbon|acetonitrile + 0.1 M electrolyte (Et_4NBF_4, Et_3MeNBF_4, $EtMe_3NBF_4$, $LiClO_4$ or $LiBF_4$) interfaces indicate that the series capacitance, series resistance, phase angle and other parameters depend noticeably on the composition of the electrolyte as well as on the electrode potential. In the region of electrode potentials $0 < E < 0.4$ V (vs. SCE in H_2O), a very well expressed differential capacitance minimum in the series capacitance vs. potential curves has been observed, with the potential of the capacitance minimum, E_{min}, equal to the total (or free) zero charge potential, dependent on the electrolyte composition. It was found that $E_{\sigma=0}$ increases in the order $LiClO_4 < LiBF_4 < EtMe_3NBF_4 < Et_3MeNBF_4 < Et_4NBF_4$, thus with the increase of adsorption

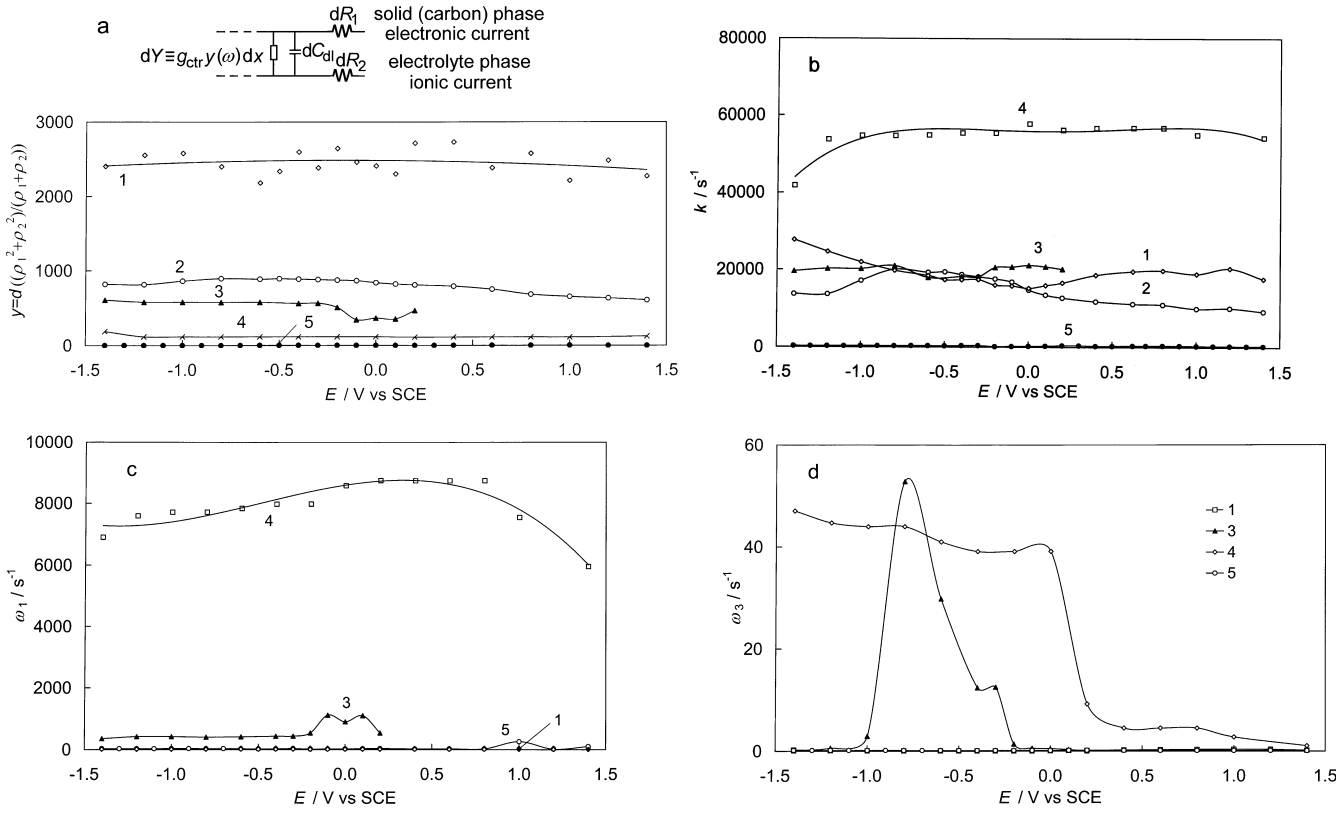

Fig. 13 **a** The dependences of the parameter $d((\rho_1^2+\rho_2^2)/(\rho_1+\rho_2))$ and the characteristic frequencies **b** k, **c** ω_1 and **d** ω_3 (calculated according to Paasch et al. model I; see Fig. 8c) on the electrode potential for nanostructured carbon ID1369 in acetonitrile solutions with addition of 0.1 M electrolyte: $LiBF_4$ (*1*), Et_3MeNBF_4 (*2*), $LiClO_4$ (*3*), Et_4NBF_4 (*4*), and $EtMe_3NBF_4$ (*5*)

activity of the cations caused by the increase of the molar mass of the cations. The values of the differential series capacitance C_s, obtained from the complex plane ($-Z''$ vs. Z') plots, depend noticeably on the a.c. current frequency if $f \geq 1\times10^{-2}$ Hz. Only at a very small a.c. current frequency is C_s practically independent of f, indicating that the nearly limiting capacitance values have been established. Non-linear regression analysis of the complex plane plots shows that the nanoporous carbon|AN + 0.1 M Et_4NBF_4, Et_3MeNBF_4 or $EtMe_3NBF_4$ electrolyte interfaces can be simulated by the equivalent circuit, in which the two parallel conduction parts in the solid and liquid phases are interconnected by the double layer capacitance in parallel with the complex admittance of the hindered reaction of the charge transfer (or partial charge transfer in our case) process, i.e. by the Paasch et al. model I [11]. The values of the characteristic frequency depend on the electrolyte composition and on the electrode potential, i.e. on the nature and structure of the ions adsorbed at the surface of the nanoporous carbon electrode. Additionally, it was found that, in the region of higher a.c. frequencies, the nanoporous carbon ID 1369|AN + 0.1 M electrolyte interface can be simulated by the modified Randles-like equivalent circuit (i.e. by the Ho et al. model [46]), where the generalized finite length Warburg element for a short-circuit terminus model has been used in spite of the classical Warburg diffusion impedance [1, 46, 47]. The complex plane plots for the nanoporous carbon ID 1369|0.1 M $LiClO_4$ (or 0.1 M $LiBF_4$) + AN interface at $E \leq E_{\sigma=0}$ can be simulated by the Meyer et al. model [48], in which the charge transfer and double layer charging at the surface, the solid phase diffusion inside the nanoparticle (i.e. nanoporous material) and the dependence of the open-circuit potential on the intercalant concentration, as well as the effect of an insulating film surrounding the nanoporous particle, have been taken into account.

Acknowledgements This work was supported in part by the Estonian Science Foundation under project no. 4568.

References

1. Conway BE (1999) Electrochemical supercapacitors: scientific fundamentals and technological applications. Kluwer/Plenum, New York, p 1
2. Lust E, Nurk G, Jänes A, Arulepp M, Nigu P, Permann L, Möller P, (2002) J Condensed Matter Phys (in press)
3. Salitra G, Soffer A, Eliad L, Cohen Y, Aurbach D (2000) J Electrochem Soc 146:2486
4. Qu D, Shi H (1998) J Power Sources 74:99
5. Pell WG, Conway BE (2001) J Electroanal Chem 500:121
6. Christen Th, Carlen MW (2000) J Power Sources 91:210
7. Bisquert J, Garcia-Belmonte G, Fabregat-Santiago F, Bueno PR (1999) J Electroanal Chem 475:152
8. Macdonald JR, Johnson WB (1987) Fundamentals of impedance spectroscopy. In: Macdonald JR (ed) Impedance spectroscopy. Wiley New York, pp 1–26
9. Roušar I, Micka K, Kimla A (1986) Electrochem Engineering, vol 2. Academia, Prague, pp 1–337

10. de Levie R (1990) J Electroanal Chem 281:1
11. Paasch G, Micka K, Gersdorf P (1993) Electrochim Acta 38:2653
12. de Levie R (1963) Electrochim Acta 8:751
13. de Levie R (1964) Electrochim Acta 9:1231
14. Keiser H, Beccu KD, Gutjahr MA (1976) Electrochim Acta 21:539
15. Keddam M, Rakomoto C, Takenouti H (1984) J Appl Electrochem 14:437
16. Randin JB, Yeager EB (1972) J Electroanal Chem 38:257
17. Gerisher H, McIntyre R, Shearson D, Storck W (1987) J Phys Chem 91:1930
18. Trasatti S, Lust E (1999) The potential of zero charge. In: White RE, Conway BE, Bockris JO'M (eds) Modern aspects of electrochemistry, vol 33. Kluwer/Plenum, New York, pp 1–216
19. Amokrane S, Badiali JP (1989) J Electroanal Chem 266:21
20. Amokrane S, Badiali JP (1991) Analysis of the capacitance of the metal-solution interface. In: Bockris J O'M, Conway BE, White RE (eds) Modern aspects of electrochemistry, vol 22. Plenum, New York, pp 1–95
21. Lust E, Jänes A, Lust K, Väärtnõu M (1997) Electrochim Acta 42:771
22. Frumkin AN, Melik-Gaikazyan VI (1951) Dokl Akad Nauk SSSR 77:855
23. Lorenz W (1958) Z Elektrochem 62:192
24. Armstrong RP, Rice WP, Thrisk HR (1968) J Electroanal Chem 16:517
25. Rammelt U, Reinhard G, Rammelt K (1980) J Electroanal Chem 180:327
26. Paasch G, Schwarzenberg M, Jobst K, Sawtchenko L (1990) Mater Sci Forum 62–64:455
27. Schneider W (1975) J Phys Chem 79:127
28. Koppitz FD, Schultze JW, Rolle D (1984) J Electroanal Chem 170:5
29. Micka K, Svatá M (1978) J Power Sources 2:167
30. Izotov VY, Strizhakova NG, Kozachkov SG, Danilin VV, Mironova AA, Maletin YA, Lust E, Arulepp M, Jänes A, Nurk G, Permann L (2002) J Power Sources (in press)
31. Arulepp M, Janes A, Nurk G, Permann L, Nigu P, Lust E (2000) Electrochemical properties of skeleton carbon materials with large surface area and controlled pore size. In: Abstracts of 51st Annual ISE Meeting, Warsaw, p 946
32. Maletin YA, Strizhakova NG, Izotov VY, Kozachkov SG, Mironova AA, Danilin VV (1996) Novel type of storage cells based on electrochemical double-layer capacitors. In: Barsukov V, Beck F (eds) New promising electrochemical systems for rechargeable batteries. Kluwer, Dordrecht, pp 363–372
33. Maletin YA, Strizhakova NG, Izotov VY, Kozachkov SG, Mironova AA, Danilin VV, Ekström T (1997) Supercapacitor stacks of high energy and power density. In: Proceedings of the 7th seminar on double layer capacitors and similar energy storage devices, Deerfield Beach, Florida, pp 1–7
34. Nurk G, Jänes A, Arulepp M, Nigu P, Permann L, Lust E (2001) Electric double layer structure at porous carbon electrodes. In: Meeting abstracts of the joint international meeting of ISE and ECS, San Francisco, abstr 1006
35. Gregg SJ, Sing KSW (1982) Adsorption. Surface area and porosity. Academic, London, p 1
36. Pell WG, Conway BE, Marincic N (2000) J Electroanal Chem 491:9
37. Ue M (1994) Electrochim Acta 39:2083
38. Gill DS (1977) Electrochim Acta 22:491
39. Lust E, Jänes A, Sammelselg V, Miidla P (2000) Electrochim Acta 46:185
40. Nurk G, Jänes A, Lust K, Lust E (2001) J Electroanal Chem 515:17
41. Gileadi E (1993) Electrode kinetics for chemists, chemical engineering, materials scientists. VCH, New York pp 291–305
42. Taylor SR, Gileadi E (1995) Corros Sci 51:664
43. Sluyters-Rehbach M, Sluyters JH (1970) Sine wave methods in the study of electrode processes. In: Bard A (ed) Electroanalytical chemistry, vol 4. Dekker, New York, pp 1–127
44. Lust E, Jänes A, Sammelselg V, Miidla P, Lust K (1998) Electrochim Acta 44:373
45. Macdonald JR () ZPlot for Windows (version 2.2) fitting program, LEVM 6.0
46. Ho C, Raistrick D, Huggins R (1980) J Electrochem Soc 137:343
47. Bisquert I, Garcia-Belmonte G, Bueno P, Longo E, Bulhoes L (1998) J Electroanal Chem 452:229
48. Meyer JP, Doyle M, Darling RM, Newman J (2000) J Electrochem Soc 147:2930
49. Song H-K, Jung Y-H, Lee K-H, Dao LH (1999) Electrochim Acta 44:3513
50. Daikhin LI, Kornyshev AA, Urbakh M (1998) J Chem Phys 108:171